Journal of Theoretical Biology 264 (2010) 1147–1158

Contents lists available at ScienceDirect

Journal of Theoretical Biology

journal homepage: www.elsevier.com/locate/yjtbi

Negative feedback of extracellular ADP on ATP release in goldfish hepatocytes: A theoretical study

Osvaldo Chara [a,b,*], Diego E. Pafundo [c], Pablo J. Schwarzbaum [d]

[a] Instituto de Física de Líquidos y Sistemas Biológicos (CONICET La Plata, UNLP, CIC), Calle 59 No. 789, c.c. 565, 1900 La Plata, Argentina
[b] Departamento de Fisiología y Biofísica, Facultad de Medicina (UBA), Calle Paraguay 2155, piso 7 (1121), Buenos Aires, Argentina
[c] Translational Neuroscience Program, Department of Psychiatry, University of Pittsburgh School of Medicine, USA
[d] IQUIFIB, Facultad de Farmacia y Bioquímica, UBA, Calle Junin 956 (C1113AAD), Buenos Aires, Argentina

ARTICLE INFO

Article history:
Received 13 September 2009
Received in revised form
9 February 2010
Accepted 15 March 2010
Available online 18 March 2010

Keywords:
Mathematical models
Extracellular ATP
Extracellular ADP
Negative feedback

ABSTRACT

A mathematical model was built to account for the kinetic of extracellular ATP (ATPe) and extracellular ADP (ADPe) concentrations from goldfish hepatocytes exposed to hypotonicity. The model was based on previous experimental results on the time course of ATPe accumulation, ectoATPase activity, and cell viability [Pafundo et al., 2008].

The kinetic of ATPe is controlled by a lytic ATP flux, a non-lytic ATP flux, and ecto-ATPase activity, whereas ADPe kinetic is governed by a lytic ADP flux and both ecto-ATPase and ecto-ADPase activities. Non-lytic ATPe efflux was included as a diffusion equation modulated by ATPe activation (positive feedback) and ADPe inhibition (negative feedback).

The model yielded physically meaningful and stable steady-state solutions, was able to fit the experimental time evolution of ATPe and simulated the concomitant kinetic of ADPe. According to the model during the first minute of hypotonicity the concentration of ATPe is mainly governed by both lytic and non-lytic ATP efflux, with almost no contribution from ecto-ATPase activity. Later on, ecto-ATPase activity becomes important in defining the time dependent decay of ATPe levels. ADPe inhibition of the non-lytic ATP efflux was strong, whereas ATPe activation was minimal. Finally, the model was able to predict the consequences of partial inhibition of ecto-ATPase activity on the ATPe kinetic, thus emulating the exposure of goldfish cells to hypotonic medium in the presence of the ATP analog AMP-PCP. The model predicts this analog to both inhibit ectoATPase activity and increase non-lytic ATP release.

1. Introduction

When cells are exposed to hypotonicity, the generated osmotic gradient across the plasma membrane causes water influx and cell swelling. Since animal cells can only expand to a certain limit before bursting, adaptive mechanisms developed to counteract cell swelling by specific regulatory mechanisms. Accordingly, most vertebrate cells challenged by hypotonic media swell but then tend to return to their initial volume by means of a process termed regulatory volume decrease (RVD). This response is mainly achieved by the net efflux of osmotically active solutes, notably K^+ and Cl^-, followed by water (Lang et al., 1988; Jakab et al., 2002).

In vertebrates hepatocytes, as in other cell types, accumulating evidence indicates that extracellular ATP is important for RVD induction (Burnstock, 2007) and that the hypotonic challenge triggers ATP release from these cells. In swollen hepatocytes from skate, turbot, trout, and humans (Ballatori and Boyer, 1997; Feranchak et al., 2000; Ollivier et al., 2006; Pafundo et al., 2004), as well as murine hepatoma cells (Roman et al., 1997), endogenous extracellular ATP (ATPe) has been shown to interact with so called P receptors (previously called purinergic, see Lazarowski et al., 2003) to trigger intracellular signaling mechanisms which ultimately lead to volume down-regulation.

In a previous study we have used goldfish hepatocytes as a model system to study how different extracellular nucleotides modulate RVD, with particular focus on ATP (Pafundo et al., 2008). We showed that RVD could be activated by ATPe in a dose dependent manner. Moreover, in swollen goldfish hepatocytes the concentration of ATPe increased rapidly to a maximum, followed by a slower decay (Fig. 1A). Experimental evidence showed this non-monotonic kinetic of the extracellular nucleotide

* Corresponding author at: Instituto de Física de Líquidos y Sistemas Biológicos (CONICET La Plata, UNLP, CIC), Calle 59 No. 789, c.c. 565, 1900 La Plata, Argentina.
E-mail addresses: ochara@iflysib.unlp.edu.ar, ochara@fmed.uba.ar (O. Chara).

0022-5193/$ - see front matter © 2010 Elsevier Ltd. All rights reserved.
doi:10.1016/j.jtbi.2010.03.022

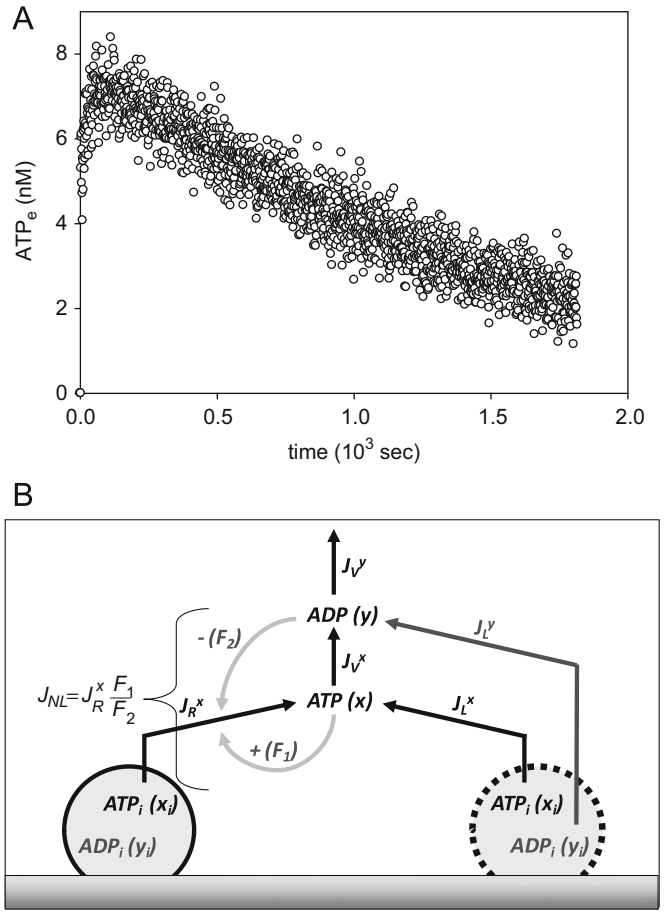

Fig. 1. (A) Experimental time course of extracellular ATP (ATPe). The data was extracted from Pafundo et al. (2008) used with permission. Levels of endogenous extracellular ATP (ATPe) concentration of hypotonically exposed goldfish hepatocytes. In this experiment 10^4 goldfish hepatocytes were exposed to 40 μL of hypotonic medium. Results are obtained from 10 independent preparations. (B) Schematic summary of the mathematical model used. J_{NL} and J_L, are non-lytic and lytic fluxes of ATP (x) and ADP (y), respectively. J_V stand for nucleotide fluxes due to ectoATPase activity (J_v^x) or ectoADPase activity (J_v^y). F_1 and F_2 correspond to the positive and the negative feedback mechanisms. x, y, x_i, and y_i denote the concentrations of extracellular ATP, extracellular ADP, intracellular ATP, and intracellular ADP, respectively.

to be consistent with simultaneous lytic and non-lytic ATP release, together with ATP depletion by extracellular diffusion and degradation by ectonucleotidases present at the cell surface. Moreover, by using a non-hydrolysable ATP analog we characterized a positive feedback mechanism whereby extracellular ATP activates a non-lytic pathway of ATP release.

Thus, in goldfish hepatocytes exposed to hypotonic media, the concentration of ATP located at the cell surface can be affected by several mechanisms interacting simultaneously in a complex way. In a first attempt to understand the relative importance of the various processes affecting the kinetic of ATPe, we developed simple data-driven models where the non-lytic release of ATP was governed by a series of forcing functions that could be activated by ATPe concentration (Pafundo et al., 2008; Chara et al., 2009). However, such a positive feedback mechanism, if unstrained, might lead to maladaptive depletion of intracellular ATP stores (Bao et al., 2004). Although in that model rapid ATPe increase was successfully counteracted by the available ATP depletion systems, recent reports using erythrocytes suggest that extracellular ADP, acting on specific P2Y receptors might initiate a negative feedback loop to oppose the ATPe-induced ATP release (Wang et al., 2005).

Considering that goldfish hepatocytes exhibit both a significant ectoATPase activity capable of generating ADP from ATP (Schwarzbaum et al., 1998), and an active P2Y system capable of mediating RVD (Pafundo et al., 2008), we developed in this study an improved mathematical model where the kinetic of ATPe is mainly regulated by a diffusive non-lytic ATP efflux that can in principle interact with an ATPe driven positive feedback loop and a negative feedback system governed by ADPe. The relative importance of these mechanisms is analyzed in detail.

This work is structured as follows. The first part of the paper describes the dynamics of ATPe concentration, ADPe concentration and cell viability.

Next, ATPe dynamic is modeled considering sources (lytic and non-lytic fluxes of ATP) and sinks (ATP consumption by ecto-ATPase activity at the cell surface) of ATPe concentration. Similarly, simulation of ADPe kinetic considered both the lytic ADP flux and ADP generation by ectoATPase activity as sources and ectoADPase activity as the main depletion mechanism.

Finally, to test whether the model can produce physically meaningful results, stability of stationary solutions was assessed.

The model was fitted to recently published experimental data of our group (Pafundo et al., 2008), and additional simulations were carried out where the parameter space was explored beyond the best fit values to experimental data.

2. Experimental results on the kinetic of ATPe concentration

The mathematical model proposed in this study requires experimental information on the kinetics of three state variables, i.e., the concentration of ATPe, the concentration of ADPe and cell viability.

Experimental results on the kinetic of ATPe concentration, ectoATPase activity (which provides a measure of ADPe generation) and cell viability from goldfish hepatocytes exposed to hypotonic medium were generated in a previous article of our group (Pafundo et al., 2008).

Here we provide a brief account of the methodology employed. All experiments were performed using intact goldfish hepatocytes. Cell viability was assessed continuously by quantitative fluorescence microscopy using calcein (Decherchi et al., 1997). A luminometer apparatus was used to quantify the ATPe concentration via light output detection of the luciferase–luciferin reaction. Coverslips with attached cells were mounted in the measuring chamber of the luminometer. At time 0, the isotonic medium was replaced by a hypotonic medium (160–170 mosM) to generate an osmotic transmembrane gradient of ~135 mOsM, and light output was monitored and quantified continuously.

Two main types of determinations of ATPe concentration were made. On the one hand, *exogenous* ATP was used to determine ecto-ATPase activity from the rate of disappearance of ATPe. Measurements of *endogenous* ATPe were performed with 40 μl of incubation medium, a condition where the medium has a height of about 100 μm. As shown by Okada et al. (2006) continuous measurements of ATP using this small volume provide similar results as the measurement of ATP at the cell surface using a surface-attached chimeric luciferase. Since in the cell model studied ATPe can only be hydrolyzed to ADPe by Ecto-ATPase activity (Schwarzbaum et al., 1998), any rate of ATPe depletion allows to calculate the simultaneous production of ADPe. The time course of light emission was transformed into ATPe concentration vs. time by means of a calibration curve.

3. Mathematical model

The mathematical model has one intracellular and one extracellular compartment. The three state variables of the model, that is, ATPe, ADPe concentrations and cell viability were denoted as x, y, and v, respectively.

Given the fact that ATP and ADP molecules can be distributed randomly in the three dimensions of the extracellular space, it is expected that extracellular concentration of these nucleotides should not be the same in each infinitesimal extracellular volume. Additionally, extracellular concentration of both nucleotides, as well as cell viability will suffer time fluctuations at each differential volume. This is why all state variables can be considered as average magnitudes, and the resulting mathematical model derived within the framework of the mean field approach (http://en.wikipedia.org/wiki/Mean_field_theory). The levels of ATPe and ADPe concentrations are linked by ectoATPase activity; both state variables are affected by the release of intracellular ADP and ATP contents that occurs during the loss of viability. The kinetic of viability, on the other hand, was considered not to depend on the time dependent changes of the nucleotides.

3.1. Dynamics of viability

Experimental results showed that cell viability changes slightly (about 2%) with the time of hypotonic exposure. Cell viability (v, in %) was expressed as

$$\frac{dv}{dt} = k_v(B_v - v) \tag{1}$$

where k_v and B_v are parameters obtained by fitting Eq. (1) to experimental data.

3.2. Dynamics of ATPe

The concentration of ATPe (x) is a state variable that can be controlled by the following ATP fluxes (Fig. 1B): (1) flux of non-lytic ATP release ($J_{NL}{}^x$), i.e., a release of ATP from the cells not involving cell membrane rupture, (2) flux of lytic ATP release ($J_L{}^x$). In this case, the loss of cell viability leads to the release of ATP to the extracellular medium, and (3) flux of ATP due to ecto-ATPase activity ($J_V{}^x$), to account for ATP conversion to ADP at the cell surface.

3.2.1. Non-lytic ATP flux

Viable goldfish hepatocytes undergo a non-lytic release of ATP ($J_{NL}{}^x$) in response to the hypotonic challenge. $J_{NL}{}^x$ was assumed to be composed of a release flux ($J_R{}^x$) modulated by two feedback processes. Since the molecular mechanisms accounting for $J_R{}^x$ have not been identified yet, we proposed in this model the simplest mechanism, i.e., simple diffusion

$$J_R^x = \left(\frac{vA_{cell}n_{cell}g_xD_{ATP}}{100\Delta x}\right)(x_i - x) \tag{2}$$

where A_{cell} is the effective area of one cell over which ATP permeates and n_{cell} the number of cells in the assay. D_{ATP} is the diffusion coefficients of ATP in water and g_x is a nondimensional parameter representing the relative diffusion coefficient of ATP across goldfish hepatocytes plasma membrane (given in D_{ATP} units). Then, the product $D_{ATP}g_x$ stands for the diffusion coefficient of ATP across the membrane. Δx *is* the depth of the compartment, v accounts for the viability, and x_i and x are the intra- and extracellular concentrations of ATP.

In goldfish hepatocytes, addition of ATPγS (a non-hydrolysable analog of ATP), activates the release of ATP following a linear function with the concentration of the analog (Pafundo et al., 2008). Assuming that ATP behaves similarly to ATPγS, we included a factor F_1 to account for a positive feedback process whereby ATPe can amplify $J_{NL}{}^x$, as follows:

$$F_1 = a_{ATP}x + b_{ATP} \tag{3}$$

The values of a_{ATP} and b_{ATP} were obtained by fitting a linear function to experimental data previously published (Pafundo et al., 2008).

Additionally, we included factor F_2 to account for a negative feedback of ADP on the non-lytic release of ATP

$$F_2 = a_{ADP}y + b_{ADP} \tag{4}$$

Then, $J_{NL}{}^x$ was modeled by a function accounting for the release of ATP ($J_R{}^x$) which is affected by a positive (F_1), and a negative (F_2) feedback mechanism

$$J_{NL}^x = J_R^x \frac{F_1}{F_2} \tag{5}$$

$J_{NL}{}^x$ applies only to viable cells, since membrane rupture gives rise to a different mechanism of ATP release as explained below.

3.2.2. Lytic ATP flux

In swollen goldfish hepatocytes, a small but nevertheless significant loss of cell viability takes place. In terms of the model, cell death leads to the release of ATP to the extracellular medium by J_L^x. This lytic flux thus depends on the time course of cell viability (v, in %). The basic assumption is that the intracellular compartment contains the total mass of intracellular ATP ($n_i{}^{ATP}$) for any given number of cells, a mass which, according to the model, is released and diluted instantly into the extracellular compartment following cell death. The lytic flux could be modeled as

$$J_L^x = -\frac{n_{cell}n_{ATP}^i}{\varepsilon 100}\frac{dv}{dt} \tag{6}$$

where n_{cell} is the number of cells seeded on the experimental chamber, and ε is the volume of this chamber; the values of all these parameters were calculated from experimental data.

Combining Eqs. (1) and (6) drives to

$$J_L^x = \frac{k_v n_{cell}n_{ATP}^i}{\varepsilon 100}(v - B_v) \tag{7}$$

3.2.3. Flux of ATP due to ecto-ATPase activity

We have previously identified and characterized ectonucleotidases present at the surface of goldfish hepatocytes which promote the hydrolysis of extracellular ATP, i.e., enzymes displaying ecto-ATPase activity (Schwarzbaum et al., 1998; Alleva et al., 2002; Pafundo et al. 2008). In the model, $J_V{}^x$ rules the flux of ATP consumption mediated by ecto-ATPase activity. The expression for $J_V{}^x$ was derived empirically after analyzing data of ectoATPase activity assayed in intact goldfish hepatocytes over an ample range of ATPe concentrations (0–5000 nM). In a first approach a hyperbolic function was fitted to experimental data

$$J_v^x = \frac{V_m x}{K_{1/2} + x} \tag{8}$$

where V_m represents the apparent maximal value of ecto-ATPase activity, and $K_{1/2}$ the ATPe concentration at which a half-maximal activity is obtained under the specific conditions of the experiment. However, since the experimentally determined concentration of ATPe lies at least 300 times lower than the $K_{1/2}$ value, J_V can be best described by a linear function of the nucleotide concentration.

Additionally, it is expected that ecto-ATPase activity will be function of cell viability. Therefore

$$J_v^x = -\theta v x \tag{9}$$

with θ being

$$\theta = \frac{V_m n_{cell}}{K_{1/2}\varepsilon}\xi \tag{10}$$

where ξ is a constant.

3.3. Dynamics of ADPe

In this model ADPe is controlled by a lytic ADP flux (ADP release upon cell rupture) and the flux due to ecto-nucleotidase activities. Since there are no reports of ADP transport across intact goldfish hepatocytes, the model does not consider any non-lytic flux for ADP. Intact goldfish hepatocytes display ecto-ATPase activity to form ADP+Pi (Schwarzbaum et al., 1998) and ecto-ADPase activity which consumes ADP (Alleva et al., 2002).

3.3.1. Lytic ADP flux

The lytic flux for ADP ($J_L{}^y$) was expressed as

$$J_L^y = -\frac{n_{cell} n_{ATP}^i y_i}{\varepsilon 100 x_i}\frac{dv}{dt} \tag{11}$$

where x_i and y_i are the intracellular concentrations of ATP and ADP. These parameters were considered to remain constant during the simulation. Then, taking into account Eqs. (1) and (11) the lytic flux for ADP can be obtained as follows:

$$J_L^y = \frac{k_v n_{cell} n_{ATP}^i y_i}{\varepsilon 100 x_i}(v - B_v) \tag{12}$$

3.3.2. Flux of ADP by ecto-nucleotidase activities

As mentioned above, this ADP flux operates in the model as a sink for ATP and a source for ADP.

Thus, the ADP flux ($J_v{}^y$) is given by

$$J_v^y = \theta v(x - f_c y) \tag{13}$$

where f_c accounts for ectoADPase–ectoATPase activities ratio.

3.4. Model development

The three model variables are controlled by the following equations:

$$\frac{dx}{dt} = J_{NL}^x + J_L^x - J_v^x \tag{14}$$

$$\frac{dy}{dt} = J_L^y + J_v^y \tag{15}$$

$$\frac{dv}{dt} = k_v(B_v - v) \tag{16}$$

Then, using Eqs. (1)–(13), Eqs. (14)–(16) can be expressed as

$$\frac{dx}{dt} = \psi_1(x,y,v) = A + Bv + \frac{Cv}{Gy+H} + \frac{Dxv}{Gy+H} + \frac{Ex^2 v}{Gy+H} + Fvx \tag{17}$$

$$\frac{dy}{dt} = \psi_2(x,y,v) = I + Jv + Kvx + Lvy \tag{18}$$

$$\frac{dv}{dt} = \psi_3(x,y,v) = M + Nv \tag{19}$$

where

$$A = -\frac{k_v n_{cell} n_{ATP}^i B_v}{\varepsilon 100} \tag{20}$$

$$B = \frac{k_v n_{cell} n_{ATP}^i}{\varepsilon 100} \tag{21}$$

$$C = -\frac{A_{cell} n_{cell} g_x D_{ATP} x_i b_{ATP}}{\varepsilon 100 \Delta x} \tag{22}$$

$$D = \frac{A_{cell} n_{cell} g_x D_{ATP}}{\varepsilon 100 \Delta x}(x_i a_{ATP} - b_{ATP}) \tag{23}$$

$$E = -\frac{A_{cell} n_{cell} g_x D_{ATP} a_{ATP}}{\varepsilon 100 \Delta x} \tag{24}$$

$$F = -\theta \tag{25}$$

$$G = a_{ADP} \tag{26}$$

$$H = b_{ADP} \tag{27}$$

$$I = -\frac{k_v n_{cell} n_{ATP}^i y_i B_v}{\varepsilon 100 x_i} \tag{28}$$

$$J = \frac{k_v n_{cell} n_{ATP}^i y_i}{\varepsilon 100 x_i} \tag{29}$$

$$K = \theta \tag{30}$$

$$L = -\theta f_c \tag{31}$$

$$M = k_v B_v \tag{32}$$

$$N = -k_v \tag{33}$$

The model has only three fitting parameters denoted as a_{ADP}, b_{ADP}, and g_x. The first two parameters govern the negative feedback of ADP on ATP release while g_x accounts for the non-lytic ATP release itself.

4. Stationary analysis

We studied the model in steady state by setting time derivatives of Eqs. (17)–(19) to 0

$$\frac{dx}{dt} = 0 \tag{34}$$

$$\frac{dy}{dt} = 0 \tag{35}$$

$$\frac{dv}{dt} = 0 \tag{36}$$

Then

$$0 = A + Bv^{ss} + \frac{Cv^{ss}}{Gy^{ss}+H} + \frac{Dx^{ss}v^{ss}}{Gy^{ss}+H} + \frac{E(x^{ss})^2 v^{ss}}{Gy^{ss}+H} + Fv^{ss}x^{ss} \tag{37}$$

$$0 = I + Jv^{ss} + Kv^{ss}x^{ss} + Lv^{ss}y^{ss} \tag{38}$$

$$0 = M + Nv^{ss} \tag{39}$$

where x^{ss}, y^{ss}, and v^{ss} are stationary solutions of the model state variables. Steady state solutions are

$$v^{ss} = B_v \tag{40}$$

$$y^{ss} = \frac{-I - JB_v - KB_v x^{ss}}{LB_v} \tag{41}$$

where I, J, K, and L are described by Eqs. (28), (29), (30) and (31), respectively, while x_{ss} shows two possible solutions:

$$x_1^{ss} = \frac{-b}{2a} + \frac{\sqrt{b^2 - 4ac}}{2a} \tag{42}$$

$$x_2^{ss} = \frac{-b}{2a} - \frac{\sqrt{b^2-4ac}}{2a} \tag{43}$$

with a, b, and c described by

$$a = 1 \tag{44}$$

$$b = \frac{\frac{A_{cell}n_{cell}g_x D_{ATP}(x_i a_{ATP} - b_{ATP})}{100\varepsilon\Delta x} - B_v^2\theta f_c b_{ADP}}{\left(\frac{A_{cell}n_{cell}g_x D_{ATP}a_{ADP}f_c}{100\varepsilon\Delta x} - \theta a_{ADP}\right)\theta B_v^2} \tag{45}$$

$$c = \frac{\frac{A_{cell}n_{cell}g_x D_{ATP}x_i b_{ATP}\theta f_c B_v^2}{100\varepsilon\Delta x}}{\left(\frac{A_{cell}n_{cell}g_x D_{ATP}a_{ATP}f_c}{100\varepsilon\Delta x} - \theta a_{ADP}\right)\theta B_v^2} \tag{46}$$

The above equations show that steady state solutions depend on fitting parameters a_{ADP}, b_{ADP}, and g_x. Thus, stationary solutions are ruled by the same three-dimensional parameters space, which control the model behavior at any time.

In an attempt to find the physical stationary solutions for the model we explored the parameters' space and discarded the imaginary and real negative values, highlighting those with physical meaning. Since x^{ss} is a function of a_{ADP}, b_{ADP}, and g_x, visualization of this function would require a four-dimensional graph. We overcome this difficulty by fixing one parameter and observing the resulting three-dimensional graph. Thus, each fixed parameter was assigned the value of best fit to experimental values (see later in Section 5). We defined an auxiliary variable, ϕ, which is 1 for each value of the parameters space generating a stationary solution with physical meaning and 0 for the remaining values.

Fig. 2A shows, for the $a_{ADP}-g_x$ space (with b_{ADP} fixed at the best fitting value) a wide area with physical meaning. It can be seen that physically meaningful stationary solutions show high density at high values of a_{ADP}, i.e. they were obtained under a strong feedback of ADPe on ATP release.

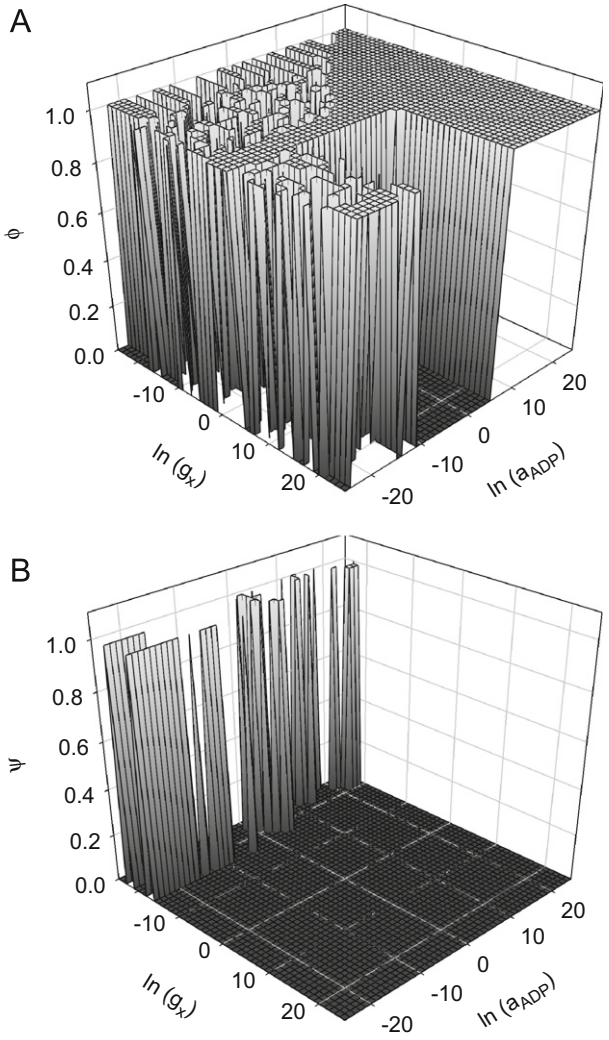

Fig. 2. (A) Steady state solutions. Stationary solutions with physical meaning over the parameters space $a_{ADP}-g_x$. ϕ is an auxiliary variable, which is 1 for each value of the parameters space generating a stationary solution with physical meaning and 0 for the remaining values. (B) Stability analysis. Stable stationary solutions over the parameters space $a_{ADP}-g_x$, where ψ is an auxiliary variable showing the cases in which the eigenvalues are complex with real part negative ($\varphi=0$) or those in which eigenvalues are complex with real part positive or zero ($\varphi=1$). a_{ADP} and g_x are non-dimensional numbers. In all cases the parameter b_{ADP} remained fixed at its best fitting value given in Table 1.

5. Linear stability analysis

Up to here we developed the model, and studied the model differential equations in steady state. In this section, we performed a linear stability analysis to test the stability of the stationary solutions. As mentioned before, the model behavior in steady state is obtained from Eqs. (34)–(36): $\psi_i(x^{ss}, y^{ss}, v^{ss})=0$ with $i=1$, 2 or 3.

In a sufficiently narrow region near the steady state, solutions of the model can be linearized to the following system:

$$\dot{X} = AX \tag{47}$$

where

$$X = \begin{bmatrix} x-x^{ss} \\ y-y^{ss} \\ v-v^{ss} \end{bmatrix}, \quad \dot{X} = \begin{bmatrix} \frac{d(x-x^{ss})}{dt} \\ \frac{d(y-y^{ss})}{dt} \\ \frac{d(v-v^{ss})}{dt} \end{bmatrix} \text{ and } \begin{bmatrix} a_{11} & a_{12} & a_{13} \\ a_{21} & a_{22} & a_{23} \\ a_{31} & a_{32} & a_{33} \end{bmatrix}$$

with $a_{i1} = \partial\psi_i/\partial x$, $a_{i2} = \partial\psi_i/\partial y$ and $a_{i3} = \partial\psi_i/\partial v$, with $i=1$, 2 or 3.

Thus, we obtain the following values for the A matrix coefficients:

$$a_{11} = \frac{DB_v + 2Ex^{ss}B_v}{Gy^{ss}+H} + FB_v \tag{48}$$

$$a_{12} = -\frac{(CB_v + Dx^{ss}B_v + E(x^{ss})^2 B_v)}{(Gy^{ss}+H)^2}G \tag{49}$$

$$a_{13} = B + \frac{C + Dx^{ss} + E(x^{ss})^2}{Gy^{ss}+H} + Fx^{ss} \tag{50}$$

$$a_{21} = KB_v \tag{51}$$

$$a_{22} = LB_v \tag{52}$$

$$a_{23} = J + Kx^{ss} + Ly^{ss} \tag{53}$$

$$a_{31} = 0 \tag{54}$$

$$a_{32} = 0 \tag{55}$$

$$a_{33} = N \tag{56}$$

Thus, by setting $\det(A-\lambda I)=0$, we obtain the following eigenvalues:

$$\lambda_1 = a_{33} \tag{57}$$

$$\lambda_2 = \frac{a_{11}+a_{22}}{2} + \frac{\sqrt{(a_{11}+a_{22})^2 - 4(a_{11}a_{22}-a_{12}a_{21})}}{2} \quad (58)$$

$$\lambda_3 = \frac{a_{11}+a_{22}}{2} - \frac{\sqrt{(a_{11}+a_{22})^2 - 4(a_{11}a_{22}-a_{12}a_{21})}}{2} \quad (59)$$

To study the stability of the stationary solutions the signs of the eigenvalues were checked. We define the auxiliary variable φ, so that for $\varphi=0$ the eigenvalues are real negative or complex with real part negative. This is the case for a stable stationary solution. In contrast, with $\varphi=1$ there is at least one eigenvalue real positive or complex with real part positive, implying stationary solutions not necessary stable. As in Fig. 2A, we fixed one parameter value to depict the effects of varying the other two fitting parameters. Fig. 2B shows the stable solutions over the parameters space $a_{ADP}-g_x$, with b_{ADP} remaining fixed at the value of best fit to experimental data obtained by Pafundo et al. (2008). Interestingly, most stationary solutions are stable.

6. Fitting the model to experimental data

6.1. Preliminary information and methods

The kinetics of ATPe and ADPe concentrations were studied in this article by mathematical modeling. For this purpose a computer program was developed that uses algorithms coded in Fortran 90 to both numerically solve the differential equations involved in each type of model and fit the model to experimental data (software and source code are available). Initially, the program was loaded with experimental data on the kinetic of ATPe concentration, substrate curve for EctoATPase activity, best fitting values of the positive feedback parameters – accounting for ATPe induced ATP release – and intracellular ATP content. To perform the simulations, Eqs. (17)–(19) were integrated numerically, employing the Euler method with an integration step of 1 s. This step guaranties the order of accuracy and the stability of the Euler method. The initial condition of the mathematical model was $x=0$, $y=0$, and $v=100\%$. This is because in the real experiments, at time 0, goldfish hepatocytes (showing an initial viability of 100%) were exposed to a hypotonic medium where ATPe and ADPe were absent (Pafundo et al., 2008).

Model dependent fit to experimental data: algebraically, the problem of fitting consists in the exploration of the free parameters space in order to minimize a given function, in this case, the sum of the squares of the residues between the experimental data of ATPe concentration and that simulated by the model under study. We called the latter procedure a model-dependent fit to emphasize the fact that during the fitting the constraints imposed by the mathematical model were taken into account. As explained in Section 2, the model is one-dimensional and has two compartments, so that ATP and ADP can be located either in an intra- or extracellular compartment (Fig. 1B). The state variables x, y, and v are ruled by Eqs. (17)–(19). Solving these equations results in a prediction of the time course of ATPe and ADPe concentrations following the hypotonic insult. Simulations were performed where the model is fitted to experimental values of ATPe concentration kinetic (Fig. 1A) by adjusting the values of the parameters a_{ADP}, b_{ADP}, and g_x.

6.2. Simulation results of the model dependent fit and preliminary predictions

Having built the model and found its stable stationary solutions we wondered whether the model could explain the experimental results. Thus, we first fitted the kinetic of one of the model variables, ATPe concentration (x), to experimental data.

The values of the fixed and fitting parameters are depicted in Table 1 with the best fitting curve shown in Fig. 3. It can be seen that the model provides a reasonable fit to experimental results.

Additionally, the model simulates the time course of ADPe concentration when the adjustable parameters are loaded with their best fitting values. According to the simulation, there is a small time shift between the maximum of both nucleotides concentrations.

Regarding the best fit simulation, it can be seen that, beyond the experimental time range assayed (between 0.0 and 1.8×10^3 s) the extracellular concentrations of both nucleotides decrease monotonically.

Table 1
Parameters of the model. Fixed parameters and initial conditions of the mathematical model (top). Results are values of best fit obtained by fitting the model to experimental time course of ATPe concentration in the absence (middle) and presence (bottom) of AMP-PCP. Experimental data from Pafundo et al. (2008) (for details of the parameters meaning see Section 3).

Model fixed parameters	**Values (units)**
k_v	0.16442041 (s^{-1})
B_v	98.00581152 (%)
n_{cell}	10,000 (cells)
D_{ATP}	0.000003 ($cm^2\,s^{-1}$)
a_{ATP}	0.00438 (no units)
b_{ATP}	0.00000000000829 ($mol\,cm^{-3}$)
ε	40 (μL)
S	3.80132711084365 (cm^2)
Δx	$\varepsilon/(2s)$ (cm)
n^i_{ATP}	7.3994×10^{-16} ($mol\,cell^{-1}$)
V_c	6.745×10^{-10} ($cm^3\,cell^{-1}$)
Cell diameter	15.44 (μm)
A_{cell}	4π (cell diameter/2)^2 (cm^2)
$V_m/K_{1/2}$	$0.0001271\,L\times10^{-6}$ ($cells^{-1}\,min^{-1}$)
ξ	1.67×10^{-7} (no units)
x_i	n^i_{ATP}/V_c ($mol\,cm^{-3}$)
y_i	(n^i_{ATP}/V_c) 0.111 ($mol\,cm^{-3}$)
f_c	1.0 (no units)
Initial conditions for the model	**Values (units)**
$x(0)$	0 ($mol\,cm^{-3}$)
$y(0)$	0 ($mol\,cm^{-3}$)
$v(0)$	100 (%)
Parameters fitted to experimental time course of ATP in the absence of AMP-PCP	**Values (units)**
g_x	0.256 (no units)
b_{ADP}	7.378×10^{-11} ($mol\,cm^{-3}$)
a_{ADP}	1.0×10^{20} (no units)
Sum of squares of residues	6.057×10^{-22} ($mol\,cm^{-3}$)
Parameters fitted to experimental time course of ATP in the presence of AMP-PCP	**Values (units)**
g_x	0.856 (no units)
b_{ADP}	8.249×10^{-11} ($mol\,cm^{-3}$)
a_{ADP}	72,446.320 (no units)
Sum of squares of residues	3.768×10^{-21} ($mol\,cm^{-3}$)

7. Exploring the space of parameters

The above considerations show the utility of the model in explaining the experimental results. In addition, it can be used to predict the kinetics of ATPe and ADPe concentrations in different scenarios. This requires new simulations where the parameters' space (Table 1) is extended beyond their best fitting values.

The model is dependent on three adjustable parameters: g_x, a_{ADP}, and b_{ADP}. As mentioned in Section 2, g_x accounts for ATP diffusion within the membrane (through an unknown structure), and a_{ADP} and b_{ADP} are parameters involving the negative feedback of ADPe concentration on ATP release. a_{ADP} represents the magnitude of ATP release inhibition by units of ADPe concentration, whereas b_{ADP} defines a basal inhibition level.

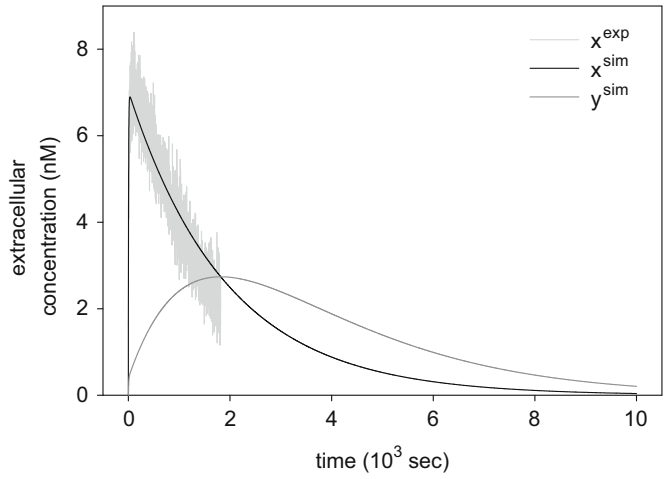

Fig. 3. Simulation of ATP and ADP kinetics. Time course of simulated extracellular ATP concentration (i.e., model dependent fit; black) fitted to experimental data (light gray), and simulated extracellular ADP concentration (gray). Experimental conditions as described in Fig. 1.

First, we studied the effect of varying g_x on the time course of both ATPe and ADPe concentrations. The results showed that the higher the value of g_x the higher the values of ATPe and ADPe concentrations at any time (Fig. 4A and B, respectively). On the contrary, when the b_{ADP} is increased, these concentrations are decreased (data not shown).

Next, we analyzed the non-monotonic ATPe concentration kinetic by considering the maximal value of ATPe concentration (ATP_e^{max}) and the time taken to reach ATP_e^{max} (t_{max}). It can be seen that, as g_x increases, ATP_e^{max} increases linearly and t_{max} decreases smoothly (Fig. 4C and D). On the contrary, when b_{ADP} increases, ATP_e^{max} decreases almost hyperbolically whilst t_{max} increases and later on saturates at about two times the best fitting value (data not shown).

Finally, by varying a_{ADP} we found that, below the value of best fit there is an explosive release of both ATP and ADP to the extracellular medium (Fig. 5A and B). In fact, as a_{ADP} decreases, both ATP_e^{max} and t_{max} increases steeply (Fig. 5C and D).

8. Analysis of the relative weight of fluxes on nucleotide dynamics

According to Section 2, the model simulates the time evolution of ATPe and ADPe concentrations based on three kinds of fluxes: lytic, non-lytic, and ectonucleotidase activities (ectoATPase and ectoADPase). Here we simulated the kinetic of the concentrations

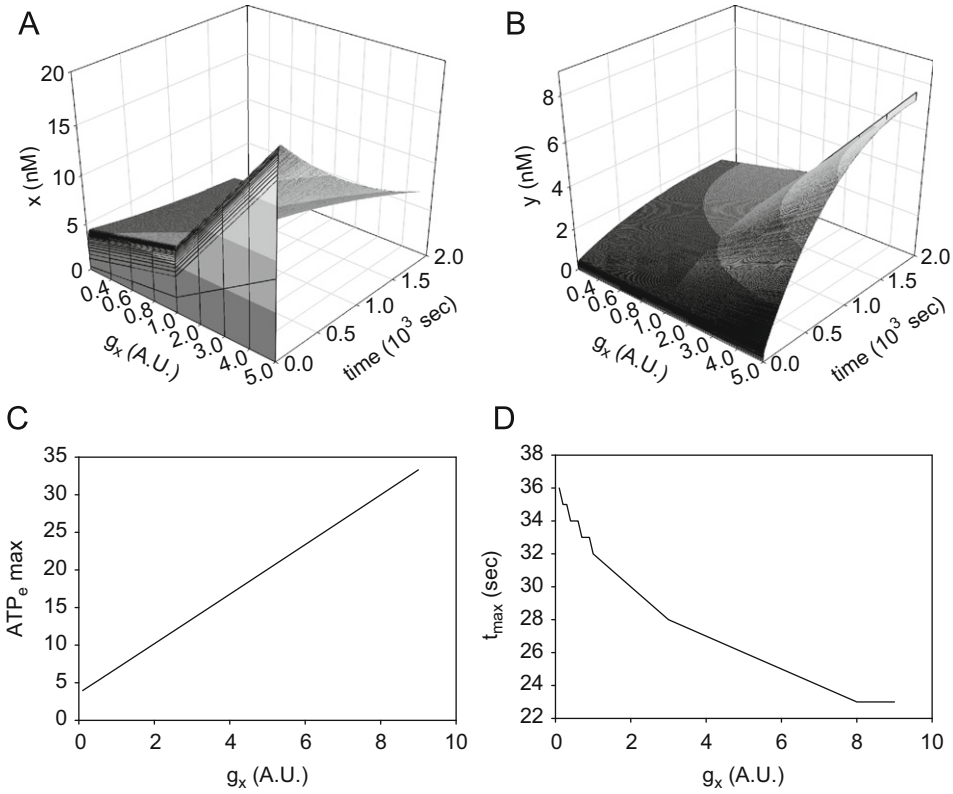

Fig. 4. Exploring the space of model parameters: relative diffusion coefficient of ATP (g_x): (A) extracellular ATP (x, nM) as a function of both time (10^3 s) and g_x (AU: arbitrary units), (B) extracellular ADP (y, nM) as a function of both time (10^3 s) and g_x (AU: arbitrary units), (C) ATP_e^{max} vs. g_x and (D) t_{max} vs. g_x. In (A) and (B) g_x ranged from 0.1 to 5 times the value of best fit; in (C) and (D) g_x ranged from 0.1 to 10 times the value of best fit. ATP_e^{max} is the maximal value of ATPe concentration (nM) and t_{max} (s) is the time taken to reach ATP_e^{max}.

of both nucleotides under a putative condition in which each of these fluxes, one at a time, is modified (Fig. 6A–F).

As expected, in the absence of lytic ATP flux, the curves describing the kinetic of ATPe (Fig. 6A) and ADPe concentrations (Fig. 6B) lie lower than the best fitting curve (denoted as Control).

Next, we studied the consequence of blocking the negative feedback of ADP on the ATP non-lytic flux, i.e., setting $a_{ADP}=0$ (Fig. 6C and D). The model predicts a strong increase of the time courses for both nucleotides. This result is consistent with those depicted in Fig. 5.

We then impose $a_{ATP}=0$ (setting a_{ADP} at its best fitting value) to block the positive feedback of ATP on ATP release, and found the resulting curve to be not distinguishable from the control one (data not shown).

Finally, by blocking ectoATPase activity alone, ATPe concentration rises to a maximum and thereafter remains constant. In contrast, after blockage of ectoADPase activity (without affecting ectoATPase activity) the simulation is not different from the control condition (Fig. 6E). Additionally, when ectoATPase is inhibited, the ADPe concentration achieves lower values than the control. On the contrary, in the absence of EctoADPase activity, ADPe shows higher values compared to the control (Fig. 6F).

9. Simulating the effects of AMP-PCP on ATP kinetic

EctoATPase activity can be inhibited by several ATP analogs such as ATPγS and β, γ-methyleneadenosine 5-triphosphate (AMP-PCP) (Joseph et al., 2003, 2004; Okada et al., 2006). Accordingly, in goldfish hepatocytes ectoATPase activity was found to decrease with increasing concentrations of AMP-PCP (0–1 mM), with maximal inhibition being 77.69% (Pafundo et al., 2008). Unexpectedly 500 μM AMP-PCP was also found to strongly enhance ATPe concentration, a result that could not be explained by ectoATPase inhibition alone and was thus compatible with stimulation of non-lytic ATP release (Fig. 7, data from Pafundo et al., 2008). Thus, we tested whether the present mathematical model could provide an explanation for this AMP-PCP induced simultaneous enhancement of ATP release and inhibition of ectoATPase activity, and the resulting changes in ATP kinetic.

To match experimental conditions a series of ATPe kinetics were simulated at 77.69% inhibition of ectoATPase activity (accounting for the observed experimental effect of 500 μM AMP-PCP) for each combination of the three fitting parameters values (a_{ADP}, b_{ADP}, and g_x).

Under this condition the model fits reasonably well to experimental data (Fig. 7), with the best value for g_x beings more than twice the control value (Table 1), whereas a_{ADP} was orders of magnitude lower than the corresponding control value (Table 1), and b_{ADP} only slightly affected (Table 1).

10. Discussion

In most hepatic cells, as in many other cell types studied so far, increases in cell volume in the face of osmotic transmembrane gradients represent the most potent stimulus for ATP release (Feranchak et al., 2000). The resulting accumulated ATPe can function as an autocrine/paracrine signal responsible for activation of cell surface purinergic receptors (Okada et al., 2001), triggering a series of intracellular events ultimately leading to osmolyte efflux and regulatory volume decrease, RVD. Although this basic model enables a qualitative explanation, a deeper insight into the ATP-induced RVD requires an understanding of the corresponding kinetic of ATPe. Thus, in this article a

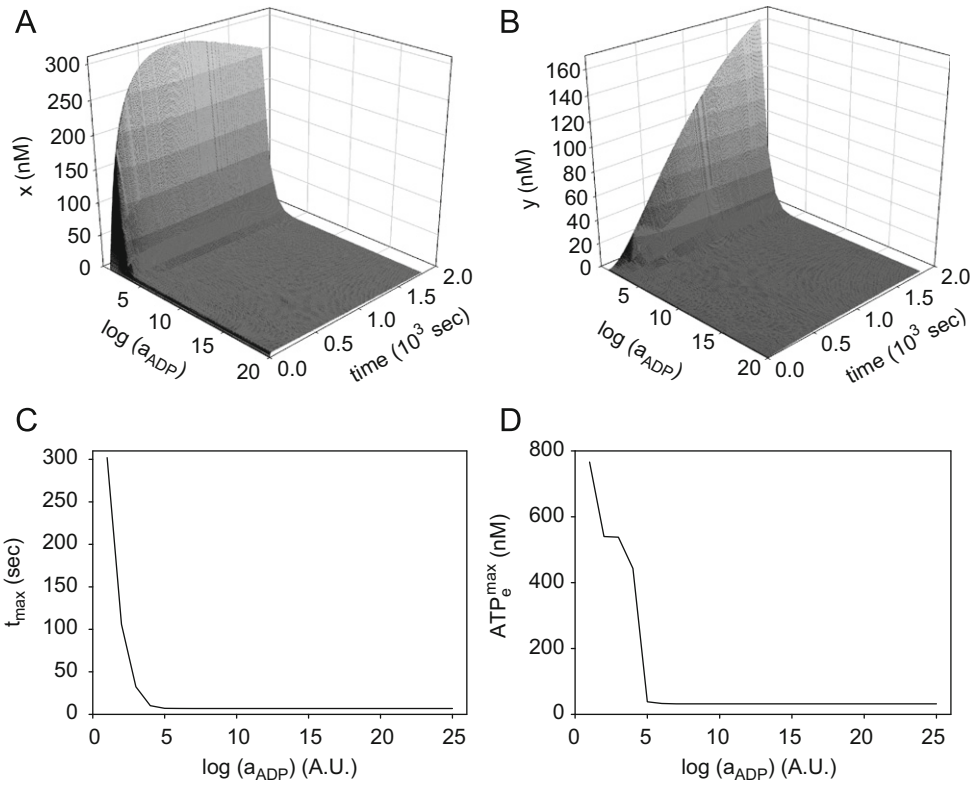

Fig. 5. Exploring the space of model parameters: negative feedback due to ADP (a_{ADP}): (A) extracellular ATP (nM) as a function of both time (10^3 s) and a_{ADP} (in arbitrary units), (B) extracellular ADP (nM) as a function of both time (10^3 s) and a_{ADP} (AU: arbitrary units), (C) t_{max} vs. a_{ADP} and (D) ATP_e^{max} vs. a_{ADP}. ATP_e^{max} is the maximal value of ATPe concentration (nM) and t_{max} (s) is the time taken to reach ATP_e^{max}. a_{ADP} is a non dimensional parameter.

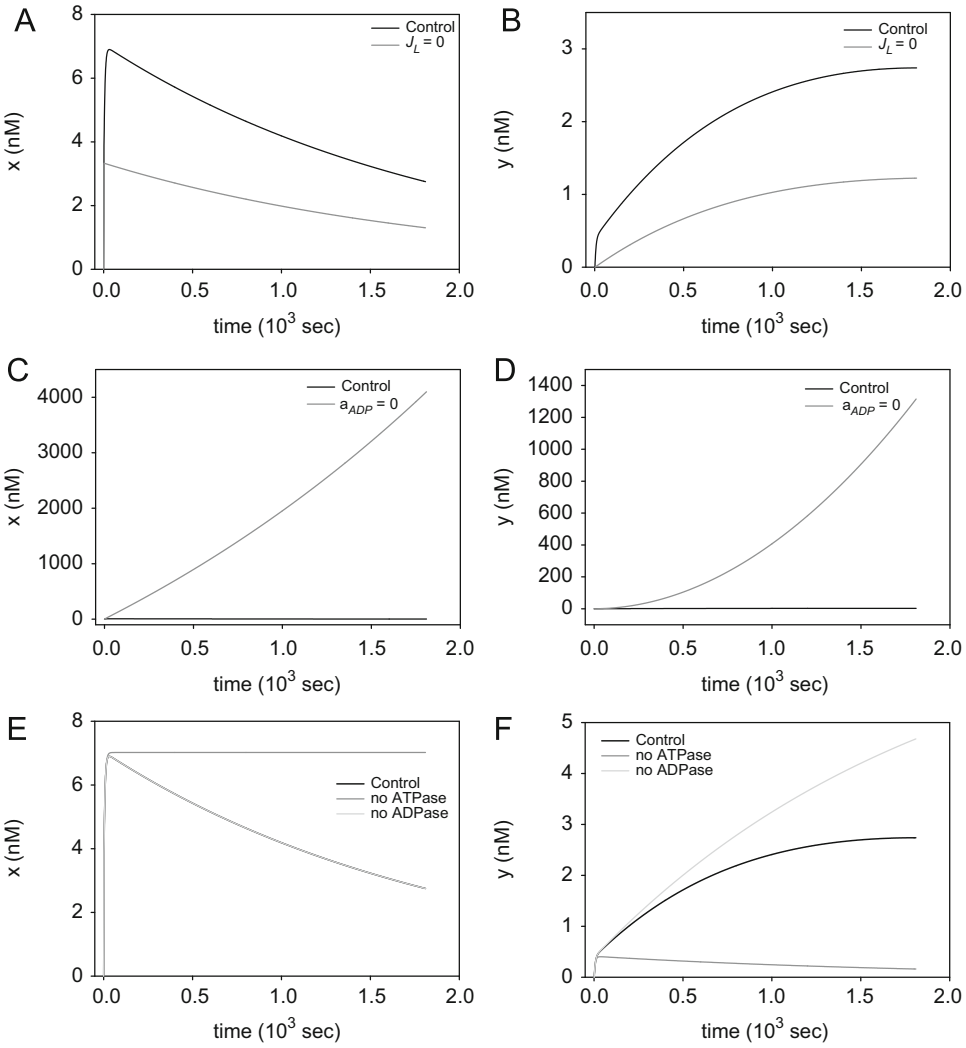

Fig. 6. Analysis of the relative effect of fluxes on nucleotide dynamics. Kinetics of ATPe and ADPe (x and y, in nM, respectively) under various conditions are shown: (A) and (B) absence of lytic ATP flux (gray) vs. control (black), (C) and (D) absence of negative feedback ($a_{ADP}=0$, gray) vs. control (black) and (E) and (F) control (black), ectoADPase blockage (no ADPase, light gray) and ectoATPase blockage (no ATPase, gray). Control condition corresponds to the best model-dependent fit to experimental data.

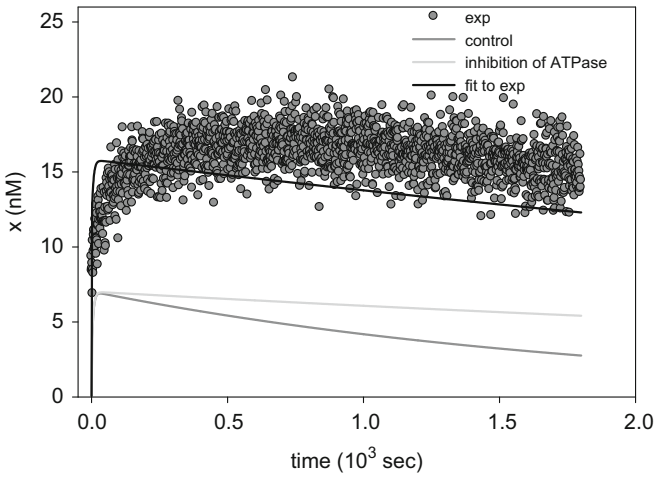

Fig. 7. Dual effect of AMP-PCP on ATP kinetic. Time course of ATPe concentration (x, nM) in control condition (control, gray curve), simulated with partial inhibition (78%) of ectoATPase activity (no ATPase, light gray curve), and fitted (fitted, continuous black curve) to experimental data (exp, dots). The data was extracted from Pafundo et al. (2008) used with permission. For experimental details see legend of Fig. 1. Control condition corresponds to the best model-dependent fit to experimental data.

mathematical model was built to explain how and why ATPe varies when hepatocytes are challenged by hypotonicity.

The model combines several features of a previous model (Chara et al., 2009) with our previous experimental data on ATPe levels, ectonucleotidase activities (measured with intact cells) and cell viability of goldfish hepatocytes (Pafundo et al., 2008). All experimental results used for modeling were obtained from the same cell model (goldfish hepatocytes), by the same group of researchers.

Experimental data showed that, following hypotonic exposure, ATPe concentration increases non-linearly to a maximum, followed by a near exponential decay (Fig. 1A). Intracellular ATP is released by lytic and non-lytic mechanisms. Once in the extracellular medium, ATP can further enhance the concentration of ATPe and at the same time be hydrolyzed to ADPe by ectoATPase activity, whereas the resulting ADPe is consumed by ectoADPase activity (Alleva et al., 2002). We have previously observed that ectoATPase activity is the main factor responsible for extracellular conversion of ATP into ADP of goldfish hepatocytes, and that neither ectoATP synthase (Mangiullo et al., 2008) nor ectophosphatase (Zimmermann, 1994) were detectable (Schwarzbaum et al., 1998).

Accordingly, in the present study all these experimental data were taken into consideration when building a mathematical

model to account for the observed ATPe kinetic of swollen goldfish hepatocytes.

The fact that in goldfish hepatocytes ATPγS increases the concentration of ATPe over an ample concentration range of the analog, and assuming that ATPγS behaves similarly to ATP, led us to propose a positive feedback mechanism whereby ATP induces the non-lytic release of ATP (Pafundo et al., 2008). This ATP induced ATP release has been suggested for other cell types as well (Anderson et al., 2004; Locovei et al., 2006). In addition, in many cell types P2Y (subtypes 12 and 13) receptor activation by ADPe has been shown to decrease AMPc (Abbracchio et al., 2006), with ATP release showing a direct proportionality to the concentration of AMPc in mammalian erythrocytes (Wang et al., 2005). Thus, to account for these findings, in our model the generated ATPe can amplify ATP release whereas progressive hydrolysis of the nucleotide produces the negative effector of that release, i.e., ADPe.

10.1. Characteristics of the model

The kinetic of ATPe is modeled by a system of autonomous and non-linear ordinary differential equations. The model includes two ATPe sources (non-lytic and lytic ATP flux) and one sink (ectoATPase activity), and two ADPe sources (ADP lytic flux and ADP generation by ectoATPase activity) and a sink (ectoADPase activity).

The non-lytic ATP efflux was modeled via a diffusion equation where ATP flux ($J_R^x$of Eq. (2)) is linearly dependent on the ATP transmembrane gradient. This is the simplest assumption considering that ATP transport mechanisms in most animal cells are not unambigously reported. That is, to date the identity of almost every ATP pore candidate (CFTR, VSDAC, connexins, and pannexins, among others) remains speculative (Praetorius and Leipziger, 2009). In general, three main mechanisms for regulated ATP release have been proposed including a conductive pore (channel), a solute transporter and exocytic release of ATP-enriched vesicles. A channel (pannexins, anion channels) would be compatible with the present model in that ATP efflux would relate directly to the ATP transmembrane gradient. An ATP transporter (e.g., ATP-binding cassette transporter proteins) could display non-linear kinetics, whereas vesicular transport will not be affected by the ATP electrochemical gradient. In the absence of molecular knowledge on ATP transport mechanisms of goldfish hepatocytes the choice of any particular model thus remains speculative, and the one chosen for Eq. (2) will be more adequate for diffusional transport mechanisms. In comparison, if other mechanisms were operative, equations describing J_R^x should turn more complex. For example, in a system where vesicular transport predominates the ATP transmembrane concentration gradient would not be considered, but other processes like Ca^{2+} mediated signaling would be taken into account.

In the model presented here three parameters exist for which no experimental information is available: g_x (the ATPe membrane diffusional coefficient), a_{ADP} and b_{ADP}. The latter two parameters are involved in the negative feedback of ADPe on the non-lytic flux of ATPe).

Before fitting the model to experimental data, we tested its stability in steady state.

By varying the values of parameters a_{ADP} (10^{-30}–10^{30}), and g_x (10^{-6}–10^{0}) a wide space of stationary solutions with physical meaning could be found, with relatively high values of a_{ADP} (Fig. 2A and B). Linear stability analysis showed that most stationary solutions were stable. Thus, physically meaningful, stable stationary solutions were found to require a strong feedback of ADPe on the non-lytic ATP release.

10.2. Model dependent fit to experimental data

Experimental results show that ATPe concentration, after attaining a maximum, decreases continuously until the nucleotide concentration is no longer significantly different from zero (Pafundo et al., 2008). The model was fitted to these results by adjusting the values of g_x, a_{ADP}, and b_{ADP}. The two parameters determining the positive feedback F_1 (i.e., a_{ATP} and b_{ATP} of Eq. (3)) were held constant at the best fitting values that were previously obtained by fitting Eq. (3) to experimental data (Pafundo et al., 2008). Model dependent fit proved reasonable, with the best fitting value for a_{ADP} being included in the solutions' space with physical meaning previously explored. After loading the parameters' best fitting values, the model generated the corresponding ADPe kinetic.

It can be seen that simulations of both nucleotides displayed a time-dependent non-linear accumulation where the maximal values are shifted, and thereafter a monotonical decrease is observed. The distribution of both nucleotides show qualitatively a similar pattern to that observed in microvascular endothelial cells from rat heart (Meghji et al., 1995), and airway epithelia (Zuo et al., 2008), depicting two non-monotonic curves characterized by two delayed maxima.

The best fitting value of g_x – accounting for ATP transmembrane diffusion – is one-tenth of the ATP diffusion coefficient in the bulk (Hubley et al., 1996), and lies in the same order of magnitude than that reported for the VDAC channel mediating ATP flow in mitochondria (Rostovtseva and Bezrukov, 1998). Moreover, this value agrees well with results on ATP flux measurements in membranes employing the luciferin/luciferase method (Rostovtseva and Colombini, 1997).

To assess the relative importance of the adjustable parameters, an exploration of the parameters' space was performed. Accordingly, we focused on how variations of g_x, a_{ADP}, and b_{ADP} affected two key empirical parameters accounting for the ATPe kinetic, i.e., the maximal value of the ATPe concentration (ATP_e^{max}), and the time taken to reach ATP_e^{max} (t_{max}). Simulations were compared with the control conditions, i.e., a condition where the model is fitted to data with the best fitting values for the three adjustable parameters.

Increases of g_x induced a linear elevation of ATP_e^{max} while t_{max} decreases smoothly. This is in principle compatible with increases in the open probability of a – yet unidentified – ATP channel (Sabirov and Okada, 2005). Since ATP_e^{max} values lie in the range of RVD activation response (Pafundo et al., 2008), higher values of ATP_e^{max} achieved at shorter times would make the RVD triggering more efficient.

Another aspect concerns the inhibitory effect exerted by ADPe (produced by ectoATPase activity and the lytic process) on the non-lytic ATP release. Interestingly, in a four-fold range around the value of best fit, the values of ATP_e^{max} and t_{max} are highly dependent on a_{ADP}. This means that in the control condition, where a_{ADP} and b_{ADP} are set to their best fitting values, negative feedback inhibition by ADPe exerts an important control on the non-lytic ATP release.

10.3. Predictions

The relative weight of each flux in determining the kinetic of ATPe and ADPe concentrations was evaluated by running the model under a condition where each of the fluxes, one at a time, is mathematically inactivated.

In goldfish hepatocytes cell death caused by swelling is small and only occurs during the first minute of the hypotonic response. One could argue that hypotonically induced cell death, even if

minor, would lead to adenylate kinase release that would affect the interconversion of adenine nucleotides in the extracellular space. However, once released to the extracellular space adenylate kinase would be exposed to nM concentrations of nucleotides, that is, concentrations at least 10^6 times below their corresponding K_m values under conditions (citrate concentration, pH, optimal Mg^{2+}:ADP, Mg^{2+}:ATP ratios) that are not optimal for enzyme activity and therefore the effect of released adenylate kinase would be negligible.

On the contrary, the effects of cell death on ATPe kinetic should not be underestimated since the intracellular nucleotide concentrations are relatively high, and, according to the model, lytic fluxes would enhance both ATPe and ADPe concentrations and at the same time contribute to both feedback mechanisms.

The consequences of these simultaneous effects can be best seen in Fig. 6A and B, where blockage of the lytic flux results in ATPe and ADPe concentrations being reduced by half over the entire time window. Although ATPe homeostasis following several environmental stimuli was studied in many different cell systems, none of them analyzed the consequences that the unavoidable cell death – even if relatively low – may exert on nucleotide kinetics. The strength of the negative feedback mechanism can be illustrated in a condition where $a_{ADP}=0$ (Fig. 6C and D). Here, the model predicts ATPe and ADPe concentrations to increase very rapidly (compared to the control condition).

Regarding the effect of the positive feedback loop, it can be seen that setting the value of a_{ATP} to 0 does not alter the simulation. Although our previous experimental data showed exogenous ATP to induce ATP release, the strength of the mechanism is relatively low in the ATPe concentration range tested. Thus, in the present model, fast acute increases in ATPe are governed by the steep ATP transmembrane gradient, with the kinetic of ATPe accumulation being modulated by a strong negative ADP feedback.

Although the inhibitory effect of ADPe on ATP efflux has been reported (Wang et al., 2005), very little is known regarding the molecular mechanisms implicated. Depending on the cell system, non-lytic ATP efflux has been shown to be triggered by changes in cytosolic Ca^{2+} (Boudreault and Grygorczyk, 2004) and AMPc (Sprague et al., 2001). The latter is consistent with ADP activating $P2Y_{13}$ receptors, which couple to Gi and decreases of AMPc (Burnstock, 2007). Alternatively, if ATP in goldfish hepatocytes was transported by pannexin 1 (an ubiquitous protein in all animal cells studied so far; Dahl and Harris, 2009), extracellular nucleotides might inhibit the channel allosterically, as suggested by Qiu and Dahl (2009).

With respect to ectonucleotidase activities, the model assumes that nucleotide concentrations – generated by the hypotonic challenge – were sufficiently low so that they behave linearly with respect to their substrates. This is a reasonable assumption since the $K_{1/2}$ for ectoATPase activity (5.7 ± 4.1 μM) is three orders of magnitude higher than the experimental ATP_e^{max} ($\sim$7 nM) and ADPe concentrations are even lower than those of ATPe. It is worth emphasizing that the $K_{1/2}$ is not the expected K_m of a single ectoATPase type, but rather reflects the concentration of ATPe which generates a half maximal ectoATPase activity (resulting by one or more ectoATPases) in an intact cell suspension. Although in certain cell types ectoADPase activity is much lower than ectoATPase activity (Wang et al., 2005; Wink et al., 2006), we have previously determined that in goldfish hepatocytes maximal ectoenzyme activities for both nucleotides were roughly similar (Alleva et al., 2002).

In Fig. 6E and F the effect of ectonucleotidases activities on ADPe kinetic were straightforward: ectoATPase activity reduced and ectoADPase increased time dependent ADPe concentrations. Interestingly, ectoATPase activity did not affect the first part of the response where ATPe achieves a maximum, but is mainly responsible for the decaying phase, so that simulating ATPe kinetic in the absence of ectoATPase activity results in ATPe concentration stabilizing at its maximal value.

The fact that ectoATPase activity does not change ATP_e^{max} prompted us to analyze previous experimental data using the non-hydrolysable ATP analog AMP-PCP. In goldfish hepatocytes exposed to hypotonic medium, AMP-PCP was found to inhibit ectoATPase activity in a dose dependent manner. Surprisingly, 500 μM AMP-PCP (which inhibit 72.2% of ectoATPase activity) enhanced the experimental ATP_e^{max} by three fold. In terms of our model, this means that the analog, in addition to inhibiting ectoATPase activity, might induce an enhancement of non-lytic ATP efflux (since no changes in cell viability were observed during this treatment). Interestingly, when human astrocytes are exposed to thrombin (to induce ATP efflux), a similar pattern of non-linear ATPe accumulation is observed (Joseph et al., 2003). Addition of AMP-PCP also produces an acute increase of ATPe in a dose dependent manner, but this analog was strictly considered – by the authors – as an ectonucleotidase inhibitor and thus its potential action as an ATP inducer was not analyzed.

Accordingly, we performed model-dependent fit to ATPe kinetic of goldfish cells in a condition where AMP-PCP (500 μM) inhibits more than 70% of the ectoATPase activity. During the fitting, the parameter space for g_x, a_{ADP}, and b_{ADP} was scanned. AMP-PCP was found to induce a two fold increase in g_x (Table 1). This is a novel finding since AMP-PCP is often used as an ectonucleotidase inhibitor but its effects on ATP efflux have not been suggested before. Moreover, AMP-PCP was shown to reduce by orders of magnitude the effect of ADP on ATP release. The molecular nature of this type of competition between ADP and AMP-PCP has not been explored yet.

10.4. Conclusions

Cells under hyposmotic shock produce a non-linear ATPe kinetic which, in turn, triggers RVD mechanisms. This time dependent pattern of ATPe accumulation is governed by several processes requiring membrane ectonucleotidases (to interconvert nucleotides), ATP transporters and extracellular nucleotides (i.e., ATPe and its byproducts). The present mathematical model provides an explanation of ATPe kinetic in terms of all these factors acting simultaneously in a complex, non-linear system.

According to the present results, the non-lytic ATP release can be described in terms of a diffusive transmembrane transport that can be activated by ATPe in a positive feedback loop and down regulated by ADP through a negative feedback mechanism. Although a few similar models were published before, none of them took the inhibitory effect of endogenous extracellular ADP on non-lytic ATP release into account.

The main findings of the present article can be summarized as follows:

- Although in goldfish hepatocytes the non-lytic ATP efflux can be activated by ATPe and inhibited by ADPe, clearly the latter mechanism prevails. This is partly due to the fact that, in the concentration range where ATPe is located, the positive feedback mechanism – unlike the negative feedback by ADPe – is weak. The immediate prediction from this analysis is that in the absence of ADPe, the modeled system would release ATP explosively. This requires an experimental verification.
- Following hypotonicity the model predicts a diffusional ATP intramembrane transport whose diffusional coefficient is in the order of that obtained in other membranes systems (Rostovtseva and Bezrukov, 1998).

- The model succeeds in interpreting complex non-linear simultaneous processes that contribute to ATPe kinetics, such as the dual action of AMP-PCP on both EctoATPase activity and non-lytic ATP efflux. In view of this novel finding, previous results on extracellular metabolism of ATP using these analogs as nucleotidase inhibitors (see e.g., Joseph et al., 2004; Okada et al., 2006; Prosdocimo et al., 2009) need to be re-interpreted.

Acknowledgements

P.J.S. and O.C. are career researchers from Consejo Nacional de Investigaciones Científicas y Técnicas of Argentina. This work was supported by grants from Consejo Nacional de Investigaciones Cientificas y Tecnicas, Universidad de Buenos Aires, and Agencia Nacional de Promoción Científica y Tecnológica (1432).

References

Abbracchio, M.P., Burnstock, G., Boeynaems, J., Barnard, E.A., Boyer, J.L., Kennedy, C., Knight, G.E., Fumagalli, M., Gachet, C., Jacobson, K.A., Weisman, G.A., 2006. International union of pharmacology LVIII: update on the P2Y G protein-coupled nucleotide receptors: from molecular mechanisms and pathophysiology to therapy. Pharmacol. Rev. 58, 281–341.

Alleva, K.E., Espelt, M.V., Krumschnabel, G., Schwarzbaum, P.J., 2002. Identification of two distinct E-NTPDases in liver of goldfish (*Carassius auratus* L.). Comp. Biochem. Physiol. B: Biochem. Mol. Biol. 131, 725–731, doi:10.1016/S1096-4959(02)00007-6.

Anderson, C.M., Bergher, J.P., Swanson, R.A., 2004. ATP-induced ATP release from astrocytes. J. Neurochem. 88, 246–256.

Ballatori, N., Boyer, J.L., 1997. ATP regulation of a swelling-activated osmolyte channel in skate hepatocytes. J. Exp. Zool. 279, 471–475.

Bao, L., Locovei, S., Dahl, G., 2004. Pannexin membrane channels are mechanosensitive conduits for ATP. FEBS Lett. 572, 65–68.

Boudreault, F., Grygorczyk, R., 2004. Cell swelling-induced ATP release is tightly dependent on intracellular calcium elevations. J. Physiol. 561, 499–513.

Burnstock, G., 2007. Purine and pyrimidine receptors. Cell. Mol. Life Sci. 64, 1471–1483.

Chara, O., Pafundo, D.E., Schwarzbaum, P.J., 2009. Kinetics of extracellular ATP from goldfish hepatocytes: a lesson from mathematical modeling. Bull. Math. Biol. 71, 1025–1047.

Dahl, G., Harris, A.L., 2009. Pannexins or connexins? In: Harris, A., Lock, D. (Eds.), Connexins: a Guide. Humana Press, Springer, New York, pp. 287–304.

Decherchi, P., Cochard, P., Gauthier, P., 1997. Dual staining assessment of Schwann cell viability within whole peripheral nerves using calcein-AM and ethidium homodimer. J. Neurosci. Methods 71, 205–213, doi:10.1016/S0165-0270(96)00146-X.

Feranchak, A.P., Fitz, J.G., Roman, R.M., 2000. Volume-sensitive purinergic signaling in human hepatocytes. J. Hepatol. 33, 174–182, doi:10.1016/S0168-8278(00)80357-8.

Hubley, M.J., Locke, B.R., Moerland, T.S., 1996. The effects of temperature, pH, and magnesium on the diffusion coefficient of ATP in solutions of physiological ionic strength. Biochim. Biophys. Acta 1291, 115–121, doi:10.1016/0304-4165(96)00053-0.

Jakab, M., Fürst, J., Gschwentner, M., Bottà, G., Garavaglia, M.L., Bazzini, C., Rodighiero, S., Meyer, G., Eichmüller, S., Wöll, E., Chwatal, S., Ritter, M., Paulmichl, M., 2002. Mechanisms sensing and modulating signals arising from cell swelling. Cell. Physiol. Biochem. 12, 235–258.

Joseph, S.M., Buchakjian, M.R., Dubyak, G.R., 2003. Colocalization of ATP release sites and Ecto-ATPase activity at the extracellular surface of human astrocytes. J. Biol. Chem. 278, 23331–23342.

Joseph, S.M., Pifer, M.A., Przybylski, R.J., Dubyak, G.R., 2004. Methylene ATP analogs as modulators of extracellular ATP metabolism and accumulation. Br. J. Pharmacol. 142, 1002–1014.

Lang, F., Busch, G.L., Ritter, M., Völkl, H., Waldegger, S., Gulbins, E., Häussinger, D., 1988. Functional significance of cell volume regulatory mechanisms. Physiol. Rev. 78, 247–306.

Lazarowski, E.R., Boucher, R.C., Harden, T.K., 2003. Mechanisms of release of nucleotides and integration of their action as P2X and P2Y-receptor activating molecules. Mol. Pharmacol. 64, 785–795.

Locovei, S., Wang, J., Dahl, G., 2006. Activation of pannexin 1 channels by ATP through P2Y receptors and by cytoplasmic calcium. FEBS Lett. 580, 239–244.

Mangiullo, R., Gnoni, A., Leone, A., Gnoni, G.V., Papa, S., Zanotti, F., 2008. Structural and functional characterization of F(o)F(1)-ATP synthase on the extracellular surface of rat hepatocytes. Biochim. Biophys. Acta 1777, 1326–1635, doi:10.1016/j.bbabio.2008.08.003.

Meghji, P., Pearson, J.D., Slakey, L.L., 1995. Kinetics of extracellular ATP hydrolysis by microvascular endothelial cells from rat heart. Biochem. J. 308, 725–731.

Okada, S.F., Nicholas, R.A., Kreda, S.M., Lazarowski, E.R., Boucher, R.C., 2006. Physiological regulation of ATP release at the apical surface of human airway epithelia. J. Biol. Chem. 281, 22992–23002.

Okada, Y., Maeno, E., Shimizu, T., Dezaki, K., Wang, J., Morishima, S., 2001. Receptor-mediated control of regulatory volume decrease (RVD) and apoptotic volume decrease (AVD). J. Physiol. 532, 3–16.

Ollivier, H., Pichavant-Rafini, K., Puill-Stephan, E., Calves, P., Nonnotte, L., Nonnotte, G., 2006. Effects of hypo-osmotic stress on ATP release in isolated turbot (*Scophthalmus maximus*) hepatocytes. Biol. Cell. 98, 427–437.

Pafundo, D.E., Chara, O., Faillace, M.P., Krumschnabel, G., Schwarzbaum, P.J., 2008. Kinetics of ATP release and cell volume regulation of hyposmotically challenged goldfish hepatocytes. Am. J. Physiol. Regul. Integr. Comp. Physiol. 294, R220–R233.

Pafundo, D.E., Mut, P., Pérez Recalde, M., González-Lebrero, R.M., Fachino, V., Krumschnabel, G., Schwarzbaum, P.J., 2004. Effects of extracellular nucleotides and their hydrolysis products on regulatory volume decrease of trout hepatocytes. Am. J. Physiol. Regul. Integr. Comp. Physiol. 287, R833–R843.

Praetorius, H.A., Leipziger, J., 2009. ATP release from non-excitable cells. Purinergic Signal. 5, 433–446.

Prosdocimo, D.A., Douglas, D.C., Romani, A.M., O'Neill, W.C., Dubyak, G.R., 2009. Autocrine ATP release coupled to extracellular pyrophosphate accumulation in vascular smooth muscle cells. Am. J. Physiol. Cell. Physiol. 296, C828–C839.

Qiu, F., Dahl, G., 2009. A permeant regulating its permeation pore: inhibition of pannexin 1 channels by ATP. Am. J. Physiol. Cell. Physiol. 296, C250–C255.

Roman, R.M., Wang, Y., Lidofsky, S.D., Feranchak, A.P., Lomri, N., Scharschmidt, B.F., Fitz, G., 1997. Hepatocellular ATP-binding cassette protein expression enhances ATP release and autocrine regulation of cell volume. J. Biol. Chem. 272, 21970–21976.

Rostovtseva, T., Colombini, M., 1997. VDAC channels mediate and gate the flow of ATP: implications for the regulation of mitochondrial functions. Biophys. J. 72, 1954–1962.

Rostovtseva, T.K., Bezrukov, S.M., 1998. ATP transport through a single mitochondrial channel, VDAC, studied by current fluctuation analysis. Biophys. J. 74, 2365–2373.

Sabirov, R.Z., Okada, Y., 2005. ATP release via anion channels. Purinergic Signal. 1, 311–328.

Schwarzbaum, P.J., Frischmann, M.E., Krumschnabel, G., Rossi, R.C., Wieser, W., 1998. Functional role of ecto-ATPase activity in goldfish hepatocytes. Am. J. Physiol. Regul. Integr. Comp. Physiol. 274, R1031–R1038.

Sprague, R.S., Ellsworth, M.L., Stephenson, A.H., Lonigro, A.J., 2001. Participation of cAMP in a signal-transduction pathway relating erythrocyte deformation to ATP release. Am. J. Physiol. Cell. Physiol. 281, C1158–C1164.

Wang, C.J., Vlajkovic, S.M., Housley, G.D., Braun, N., Zimmermann, H., Robson, S.C., Sevigny, J., Soeller, C., Thorne, P.R., 2005. C-terminal splicing of NTPDase2 provides distinctive catalytic properties, cellular distribution and enzyme regulation. Biochem. J. 385, 729–736.

Wink, M.R., Braganhol, E., Tamajusuku, A.S., Lenz, G., Zerbini, L.F., Libermann, T.A., Sevigny, J., Battastini, A.M., Robson, S.C., 2006. Nucleoside triphosphate diphosphohydrolase-2 (NTPDase2/CD39L1) is the dominant ectonucleotidase expressed by rat astrocytes. Neuroscience 138, 421–432, doi:10.1016/j.neuroscience.2005.11.039.

Zimmermann, H., 1994. Signalling via ATP in the nervous system. Trends Neurosci. 17, 420–426.

Zuo, P., Picher, M., Okada, S.F., Lazarowski, E.R., Button, B., Boucher, R.C., Elston, T.C., 2008. Mathematical model of nucleotide regulation on airway epithelia. Implications for airway homeostasis. J. Biol. Chem. 283, 26805–26819.